NRIAG JOURNAL OF ASTRONOMY AND GEOPHYSICS
2021, VOL. 10, NO. 1, 279–289
https://doi.org/10.1080/20909977.2021.1915080

Taylor & Francis
Taylor & Francis Group

ARTICLE

Enhancement the VES models based on the TEM measurements and the application of static shift corrections.: case study from Egypt

Manal M. Osman[a], Gad M. El-Qady[b], Th Abdel Fattah[a], M Rashed[a] and M. Mohamdeen[c]

[a]Geology Department, Faculty of Science, Alexandria University, Alexandria, Egypt; [b]National Research Institute of Astronomy and Geophysics (NRIAG), Helwan, Egypt; [c]National Institute of Oceanography and Fisheries, Alexandria Branch, Egypt

ABSTRACT

Variations in conductivity in the near-surface, such as the presence of small and localized three-dimensional (3D) bodies, cause a galvanic distortion in direct current (DC), so the measured apparent resistivity is affected by a constant shift on a log scale called Static Shift. In this study, We used electromagnetic sounding techniques to correct for the static shift affecting the electric resistivity data only. The term "static shift" is used because apparent resistivity is distorted by a constant, shifting value (S) on a log scale, which lead to misleading interpretation. It was noticed that the two data sets' sounding curves at the same location have a concordant pattern. The problem was noticed in the 1D inversion models for VES and TEM were not matched together before removal of VES data shift. The TEM and VES measurements are represented on the same graph, then the shifting factor (S) is calculated for the VES curves to directly overlap the TEM curve. The 1D inversion model for VES curves after removing the shifting factor shows matched data with the TEM 1D model.

ARTICLE HISTORY
Received 6 October 2020
Revised 2 April 2021
Accepted 7 April 2021

KEYWORDS
Shalateen; resistivity; tem; static shift

1. Introduction

Vertical electrical sounding and transit time electromagnetic methods are among the leading methods in the exploration geophysics and management of groundwater (Zohdy et al. 1974; Zohdy 1989; Massoud et al. 2009). Differences between geologic environments and subsurface conditions lead to applying different geophysical techniques to solve the subsurface geologic problems in an integrated manner. Integration between geophysical methods may solve such a problem using proper algorithms (Barker 1981; Park 1985; Sternberg et al. 1988; Bahr 1988, 1991; Barker 1992; Beard and Tripp 1995; Spitzer 2001). Variations in conductivity in the near-surface caused by small and localised three-dimensional (3D) bodies cause the electric charges' build-up across near-surface inhomogeneities. This, in turn, will cause a galvanic distortion (static shift) in direct current (DC) electric resistivity methods. This leads to distortion of the apparent resistivity curves leading to an inaccurate interpretation (Pellerin & Hohmann 1990 and Stephen et al. 2003). The static-shift effect, which leads to incorrect estimation of resistivities and erroneous modelling of the subsurface, should be resolved using a wide variety of approaches (Delhaye et al. 2017).

The aim of this paper is to put together the electric and TEM depth sounding curves for accurate identification and removal of static shift factor (S) in the DC sounding curves. The removal of the static shift produces more proper profiling of subsurface resistivity and structure. The TEM sounding curves were represented with the DC sounding curves on the same log-log graph using (Meju 2005) method. Both have a concordant pattern, but the resistivity sounding curve is shifted upward or downward form the TEM curve. The shifting factor (*S*) is calculated for each VES, allowing all points along the VES sounding curve to be directly overlapped with the TEM curve.

2. Study area and geological setting

The coastal fan in the Shalateen area (Figure 1) represents a good case study for the static shift in vertical electric sounding caused by geological heterogeneity in the near subsurface layers. The study area lies along the Red Sea coast at the Northern corner of the Halayieb – Shalateen triangle.

Coral reefs and raised beaches represent the exposed deposits dominate along with some parts of the coast. Moreover, gypsum and Nubian sandstone of the Upper cretaceous age dominate along some portions in the west (Yehia et al. 2006; Yousef et al. 2009). Nubian sandstone refers to Abu Aggag Formation and formed from cross-bedding and laminated medium to fine sandstone intercalated with silt and clay (Yousef et al. 2009).

Three main groups represent the Post-Nubian deposits; the first one is the Carbonate group, consisting of limestone of Upper Cretaceous (150–700 m

CONTACT Manal M. Osman geo.manalosman@gmail.com Geology Department, Faculty of Science, Alexandria University, Alexandria, Egypt

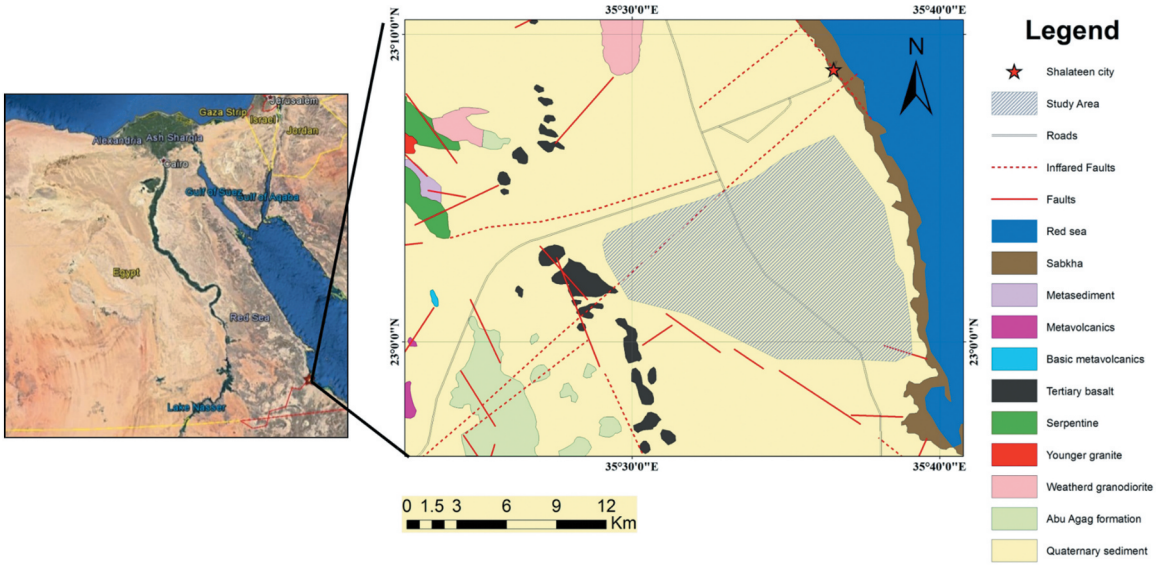

Figure 1. Geologic map of the study area (combined after Conoco map, 1981 and Sadek 2008).

thick). The carbonate rocks are nonporous but contain fissures, fractures, and joints which act as groundwater conduits; the second group is represented by the Miocene sediments and exposed in the Red Sea coastal belt consists of evaporites intercalated with clay and sand in its upper part, and of sandstone interbedded with clay in its lower part. The thickness of this group varies from place to place (Said 1962; El-Belasy 1994; Baraka 2003). The Pleistocene Alluvial deposits represent the third group and formed of wadi fillings distributed in various depressions, over alluvial fans along with alluvial courses, and coral reefs and beach deposits.

3. Methodology and data acquisition

Integration of data from the electrical and electromagnetic (EM) sounding techniques is critical. The direct current resistivity method is based on injecting a direct current into the ground using two current electrodes (A and B) and measuring the potential difference between two potential electrodes (M and N). In comparison, the TEM method is based on a time-varying current pass into a transmitter loop, usually (wire laid on the surface). The transmitter loop generates an EM wave that propagates into the subsurface. When the EM energy encounters subsurface

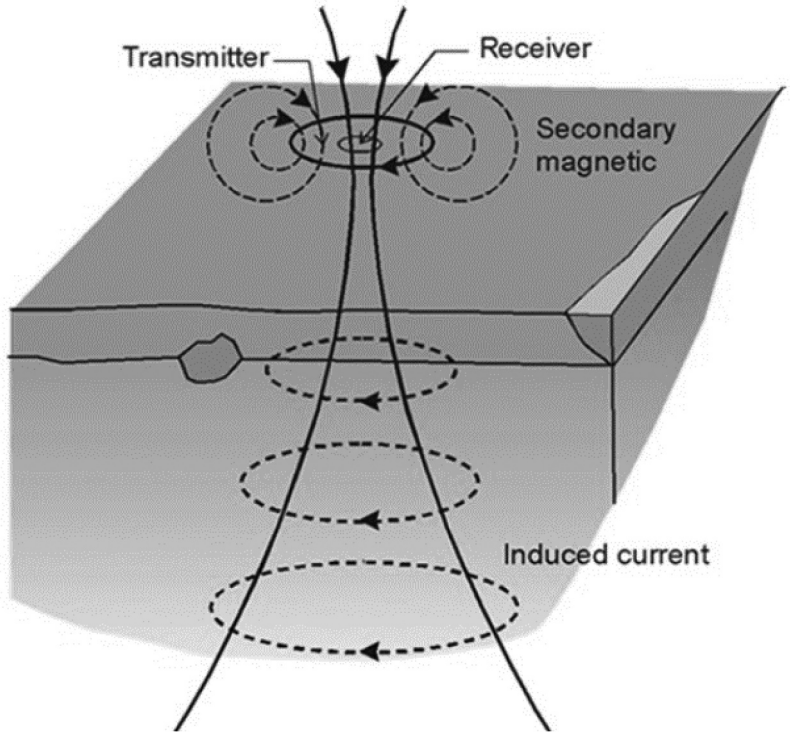

Figure 2. Transient current flow in the ground (After Hersir and Björnsson 1991).

materials of different resistivities, it induces eddy currents that generate secondary EM fields. These secondary EM fields detected at the surface by a receiver loop and recorded as the induced energy diffuses into the earth (Figure 2). The rate of diffusion indicates the resistivity of the subsurface materials (Mwakirani et al. 2012; and Bortolozo 2015), integrated VES and TEM data show concordant response patterns, Vertical Electrical Sounding (VES) is sensitive to resistive medium, while Transient Electromagnetic sounding (TEM) is sensitive to conductive medium (Sultan and Santos 2009). Moreover, VES is better for detecting shallow subsurface layers, while TEM soundings detect the deeper layers. These differences demonstrate the need for an integrated approach for using each of them for subsurface investigations.

During field acquisition of the VES soundings, Schlumberger array was used, and the current electrode spacing is increased logarithmically (maximum AB/2 between 250 m and 300 m) at nearly equal increments (7 points at each cycle) to get more depth. The distance between the potential electrodes is held fixed for the succession measurements. Then, the distance between the potential electrodes is increased. The apparent resistivity is calculated at each current-electrode spacing using the Schlumberger equation (Figure 3). All field survey precautions were considered (Flathe 1976; Flathe and Leibold 1986). The sounding curves were drawn on a log-log scale during a field survey to avoid any possible readings error. The VES data are shown as apparent resistivity versus electrode separation (Figure 4).

Transient electromagnetic (TEM) surveys were conducted in the studied area using Sirotem MK3 conductivity metre, where the stations are distributed along with the VES locations. Stations location is selected to be away from any external electrical source or high potential lines to minimise the noise effect. The square lope size used during acquisition was 50 m. At some stations, the field measurements were repeated two or three times with different acquisition parameters to assure good data quality. The data are presented as apparent resistivity versus transient time (Figure 5). The study area has been covered by 11 VES stations and 11 TEM stations distributed along with the profiles parallel to the shoreline and one random (Figure 6).

Static shift on the apparent resistivity curve may be caused by shallow or near-surface conductivity heterogeneity due to local geology. As the TEM measures the decaying field and not the electric current (Tang et al. 2018), so the TEM sounding is not affected by the static shift, and then can be used for static shift correction for resistivity data.

In the Meju (2005) experiment, the geological model was characterised by a conductor of low resistivity layer between two relatively highly resistive layer. Those conditions are quite similar to the current study, where the saltwater aquifer represents the conductive layer. He determined empirically (from numerical modelling and field studies of collected DC resistivity and TEM depth soundings in different environments) the apparent-resistivity data from transient electromagnetic and steady-state electrical soundings with the popular symmetric in-line 4-electrode using the relationship in equation 1,

$$t = 0.5\pi\mu_0\sigma L2 \tag{1}$$

or

$$L = 711.8\sqrt{t\rho} \tag{2}$$

where the transient time t is in seconds, μ_0 is the magnetic permeability (taken to be equal to that of free-space: $\mu_0 = 4\pi \times 10 - 7$ _s/m), L is one-half the electrode spacing, and ρ (= $1/\sigma$) is the homogeneous

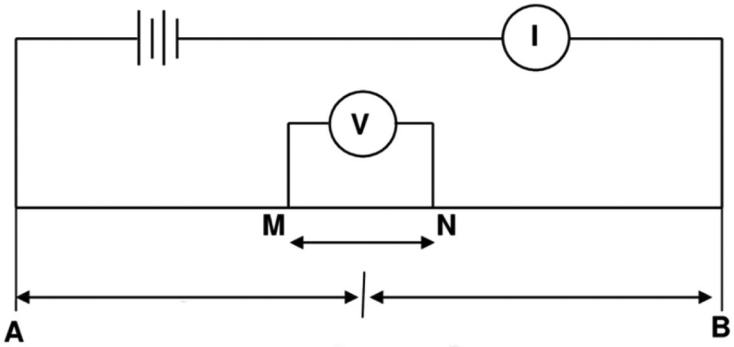

$$P=\pi \frac{(AB/2)^2-(MN/2)^2}{MN}\frac{\Delta V}{I}$$

AB/2 = half current electrode spacing.

MN/2 = half potential electrodes spacing.

ΔV = potential difference measured between the potential electrodes M and N,

I = electric current injected into the ground by the current electrodes A and B.

Figure 3. Schlumberger array distribution and equation.

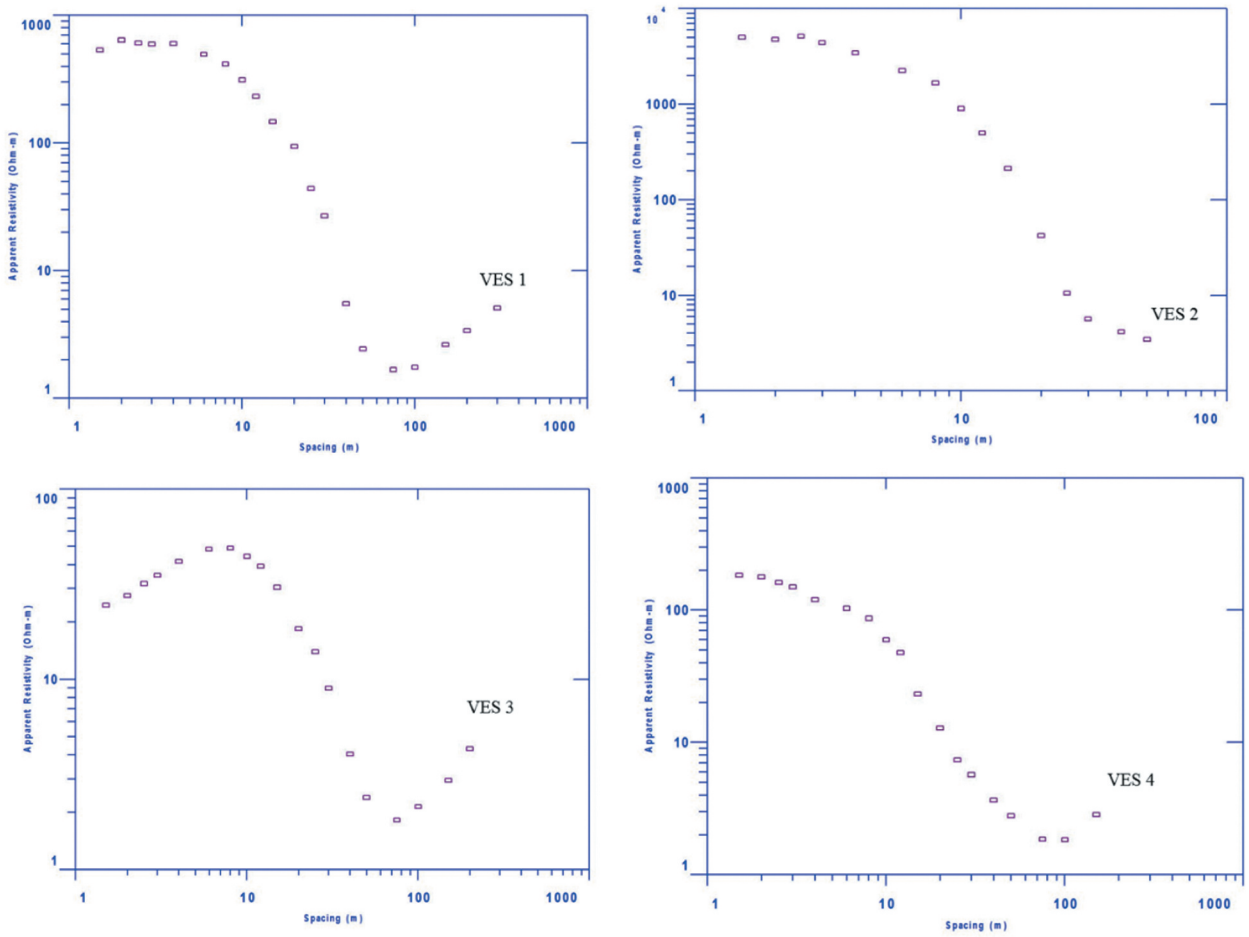

Figure 4. Sounding curves of VESs (1,2,3,4) as it is represented as apparent resistivity Vs half electrode separation.

subsurface resistivity (in Ωm), which is only known after data inversion and so conveniently approximated here by the apparent resistivity ρa to be matched with field data.

After applying equation (2) (Meju 2005; Sultan and Santos 2009) to TEM measurements, it can be represented with the DC sounding along the same log-log graph of the apparent resistivity versus half electrode spacing. The static shift appears in the electrical resistivity sounding curve as it is shifted vertically above or below the TEM curve, but both have the same pattern (in the log domain). Static shift corrections are made by calculating the shifting factor (S) using equation (3) to match the overlapping between TEM and VES sounding curves at the unchanged curve segments.

$$\rho_a(\text{corrected}) = \rho_a(\text{measured}) * (S) \qquad (3)$$

Where ρ_a(corrected) is the apparent resistivity value after applying static shift correction, ρ_a is the measured apparent resistivity value, and S is the estimated shifting factor. The shifting factor (S) is estimated for a single point along the VES sounding curve through manual iteration. By applying this factor, the VES sounding curve's point will be directly overlapped with the TEM curve (many factors are used, and the factor that gives the best overlapping is chosen). Finally, this estimated (S) is applied for all points along the measured VES curve.

4. Results and discussions

After acquiring VES and TEM data, both data sets entered into IX-1D software for 1D inversion. It was noticed that sounding curves for the two data sets at the same location have the same curve pattern (concordant pattern), especially in the middle part of the curve. The problem arises from the 1D inversion models for VES and TEM were not matched together for the same location (Table 1). Using equation (2) for TEM measurements allows for representing it as a function of apparent resistivity with electrode spacing and hence can be represented with VES data in the same graph (Figures 7, Figures 8, and Figures 9). Matching in the curve pattern increases as the depth increases because of the vertical resolution difference between both methods, where TEM vertical resolution increases with depth. Some VES curves (VESs 1, 7) are not matched with the TEM curves in the upper part of the curve, referring to the difference in vertical resolution in the shallow parts between the two methods. The VES curves show shifting upward or downward

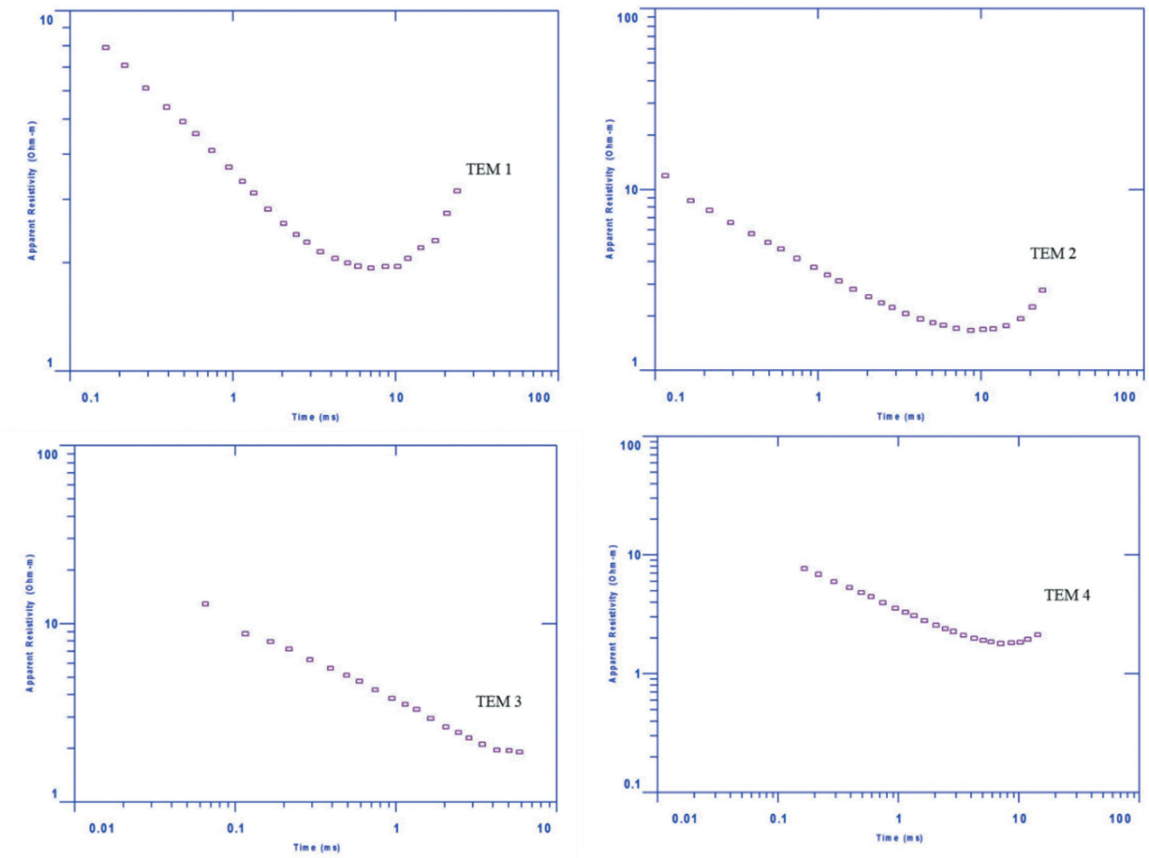

Figure 5. Sounding curves of TEMs (1,2,3,4) it is represented as apparent resistivity Vs time.

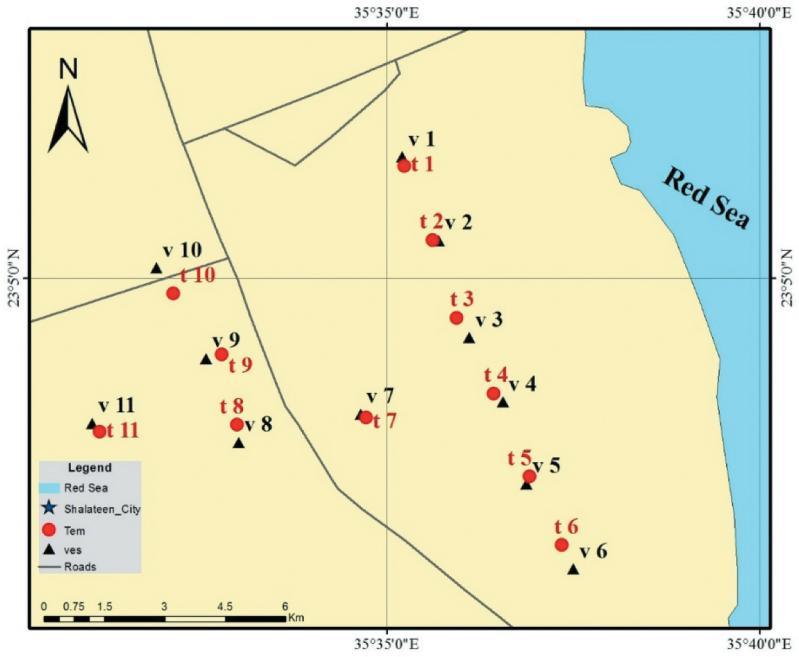

Figure 6. VES and TEM Location Map.

from the TEM curves, explaining the differences in the 1D models obtained after inversion.

We have calculated the static shift factor for all points along each VES curve by estimating the number that can be multiplied by resistivity values of all VES sounding curves that will directly overlap with the corresponding TEM curve. Figures 10,Figures 11, and Figures 12 show VES and TEM curves after

Table 1. Comparing 1D model parameters before and after removing static shift value.

		Model before shift		Model after shift		TEM Model
VES & TEM No.	Static Shift Value (s)	Surface layer resistivity	Basement depth	Surface layer resistivity	Basement depth	Basement depth
v1, t1	0.22	2674.8	94.939	588.46	91.833	90.476
v2, t2	2.3	2249.6		5277.4		91.479
v3, t3	0.012	1841.1	32.342	17.688	98.962	90.497
v4, t4	0.14	1356.4	62.001	192.92	91.833	91.66
v5, t5	0.5	408.06	56.54	214.9	91.833	90.542
v6, t6	0.03	1302		38.992		
v7, t7	0.07	3162.2		227.22		92.667
v8, t8	0.035	60.515		66.82		82.136
v9, t9	0.018	3451.1	40.765	65.452	94.102	92.583
v10, t10	0.09	1040.7	52.01	93.74	90.657	91.86
v11, t11	0.08	1505.6		121.98		99.038

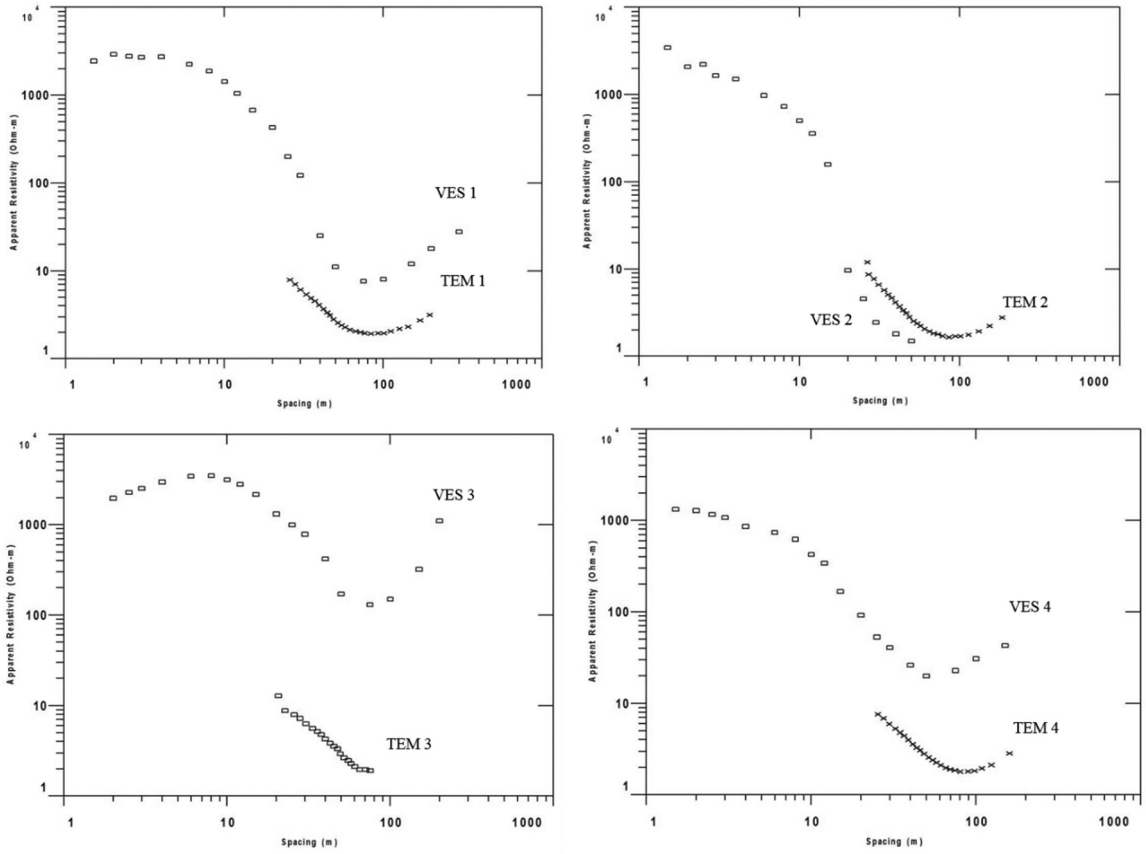

Figure 7. VES and TEM sounding (1,2,3,4) curves before static shift.

applying the static shift factor values (VES and TEM curves overlapped). The static factor value varies between 0.014 and 2.15 for the different VESs.

After correction of VES data to the static shift factor, a 1D model is prepared, which is used as an initial model for TEM data inversion. Both VES and TEM curves are processed using the same algorithm (IX1-D v3) (IX1D v3 Instruction Manual, 2008). This approach allows using the same assumptions for VES and TEM and also using the equivalence concept. To compare the static shift's effect on the subsurface earth model's interpretation, the shifted 1D VES inversion models were highly matched with TEM models (Table 1), compares the results obtained before and after shift. This table shows that the basement rock in Shalateen was at a depth of 49 m before removing the shifting value, which is not matched with the study area's geology and previous studies. After applying the static shift, the basement was interpreted to be at a depth of 91 m, matching with geology and the 1D model of TEM station at the same location.

Figure (13) shows a contour map for variation in static shift factor in the study area. The static shift factor decreases westward, where the basement rock exists at shallow depths and increases eastward because of the salt water intrusion. This, in turn, indicates that the saltwater intrusion and the depth to basement rocks significantly affect the measured data. Moreover, the saltwater intrusion increases to the east, causing an increase in the saltwater bearing layer eastward. Increasing the thickness of the saltwater body causes an increase in the distortion of the

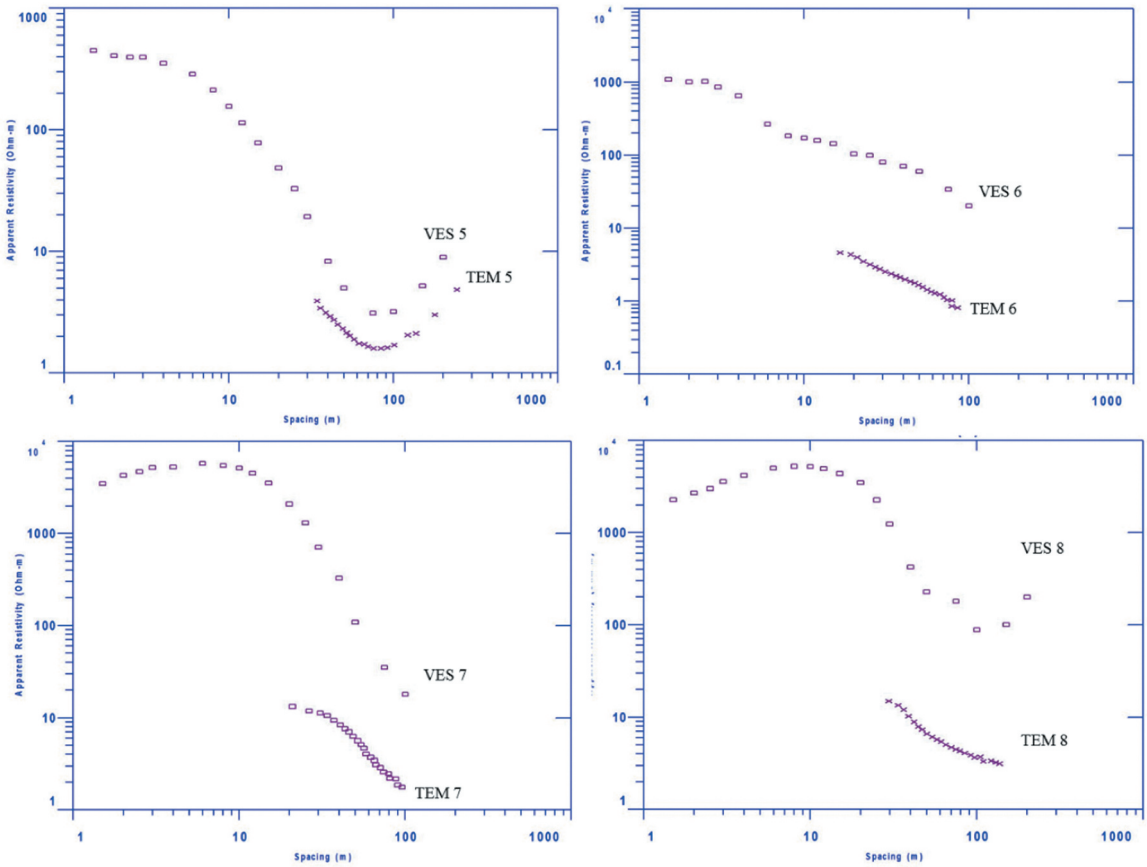

Figure 8. VES and TEM sounding (5,6,7,8) curves before static shift.

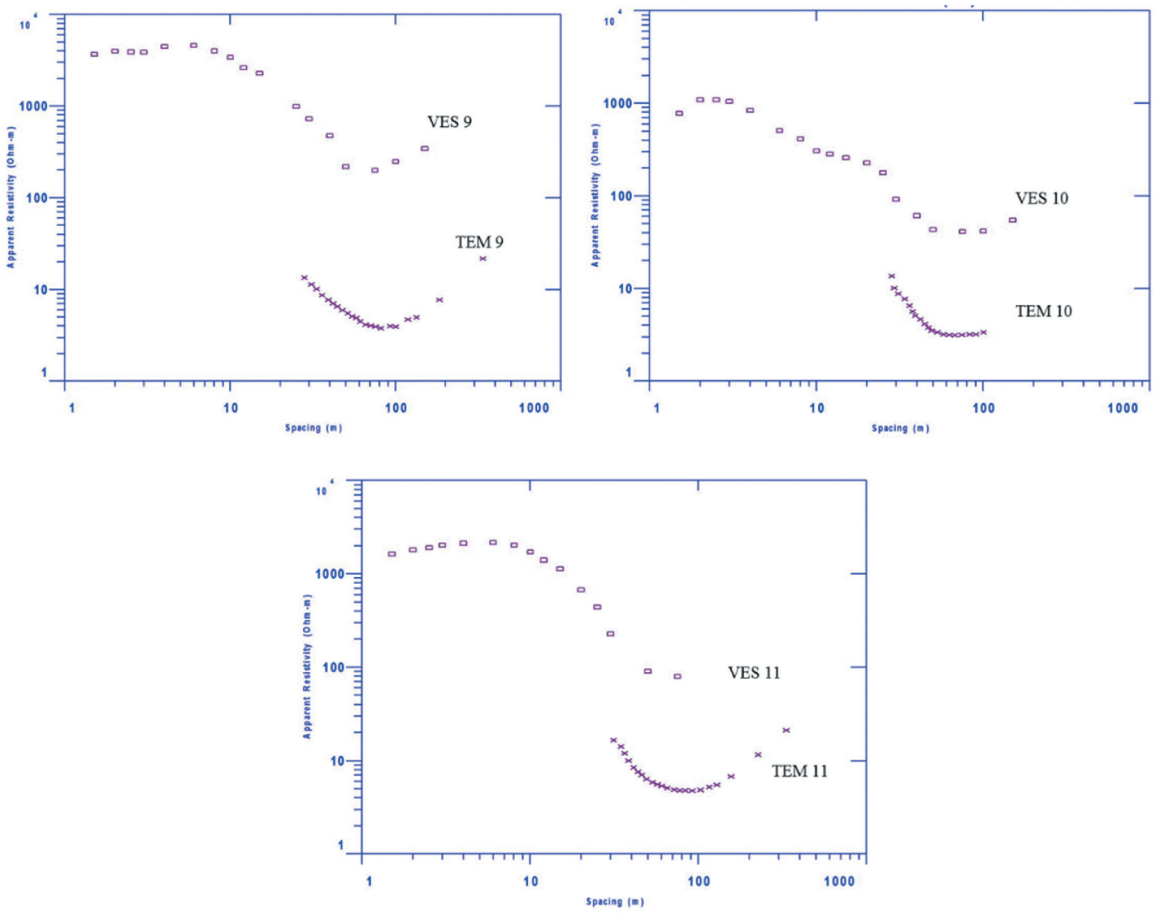

Figure 9. VES and TEM sounding (9,10,11) curves before static shift.

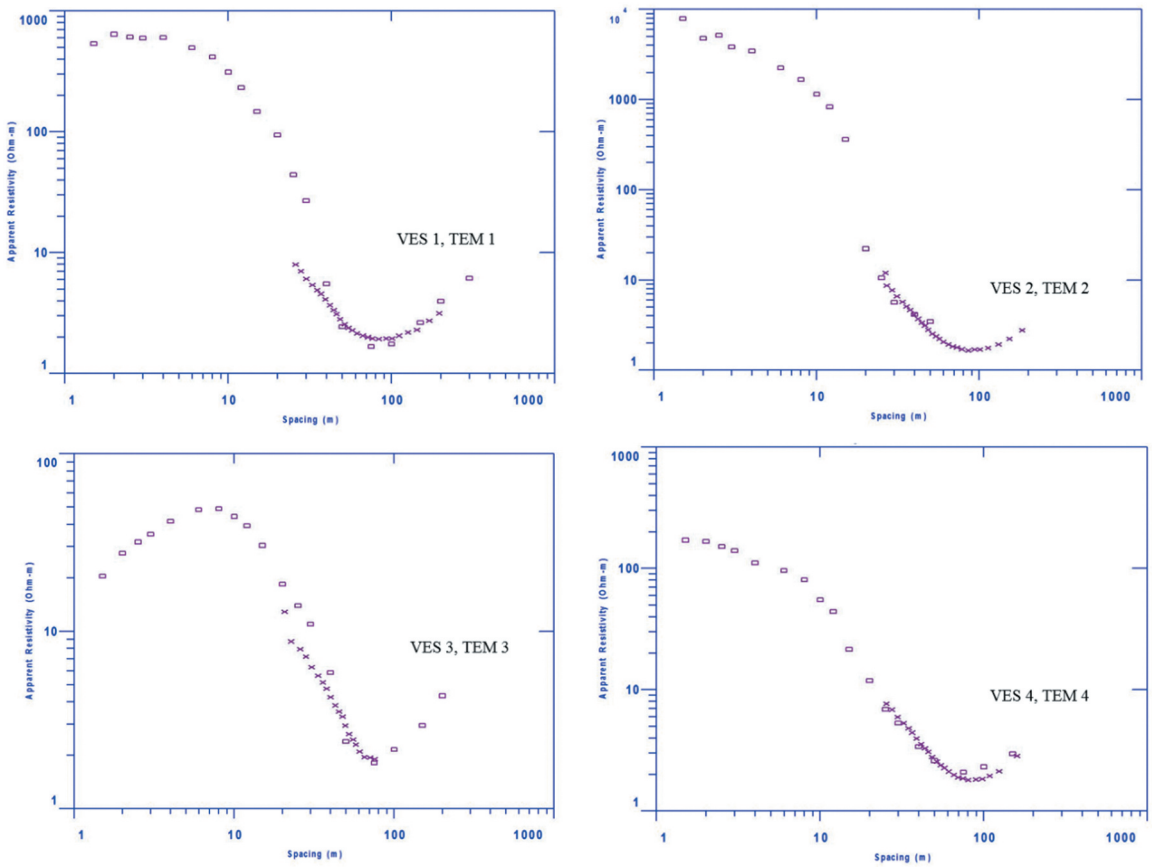

Figure 10. VES and TEM sounding (1,2,3,4) curves after static shift.

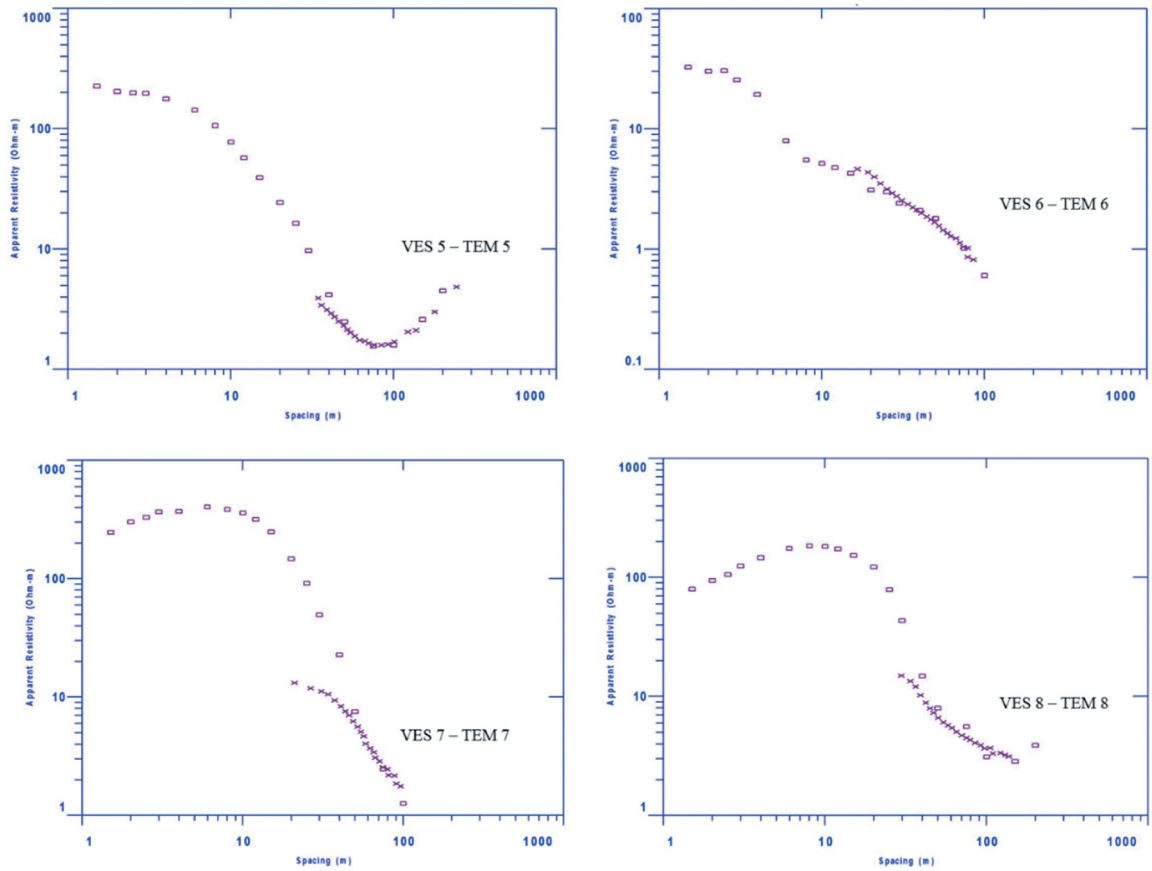

Figure 11. VES and TEM sounding (5,6,7,8) curves after static shift.

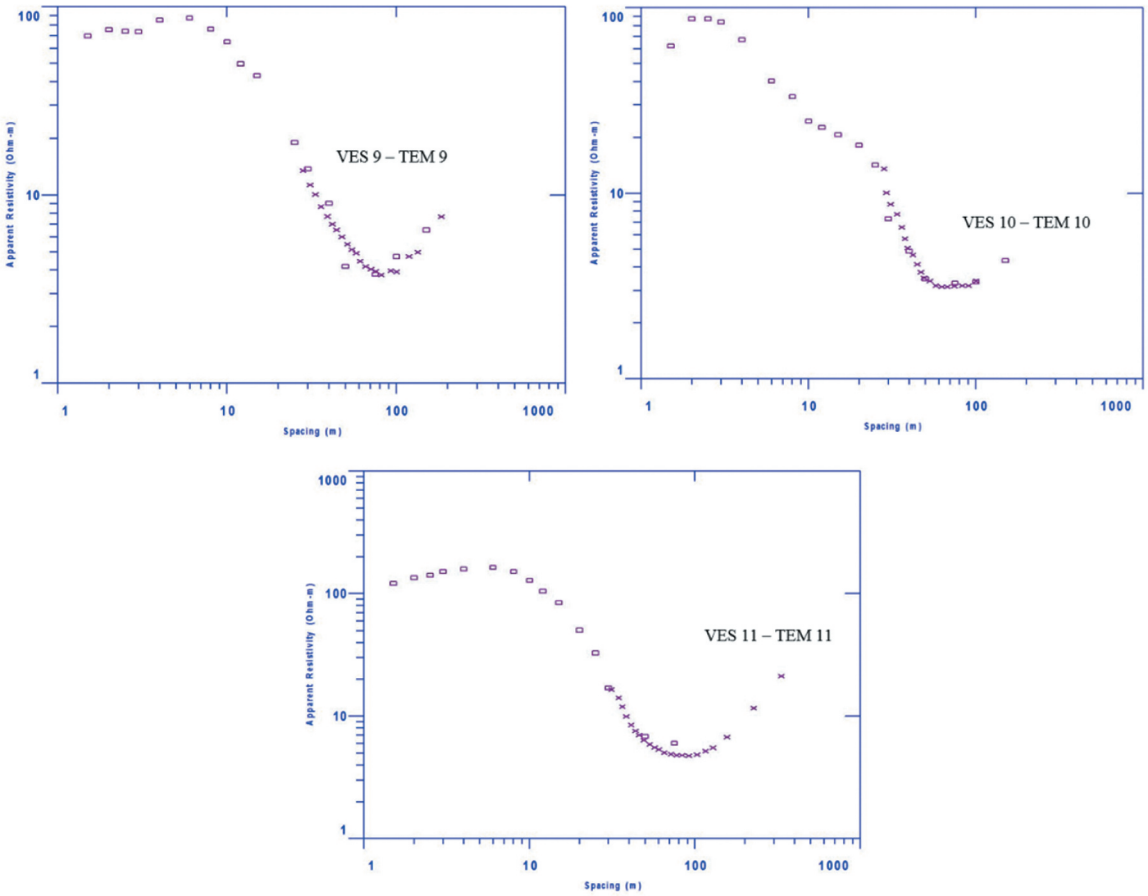

Figure 12. VES and TEM sounding (9,10,11) curves after static shift.

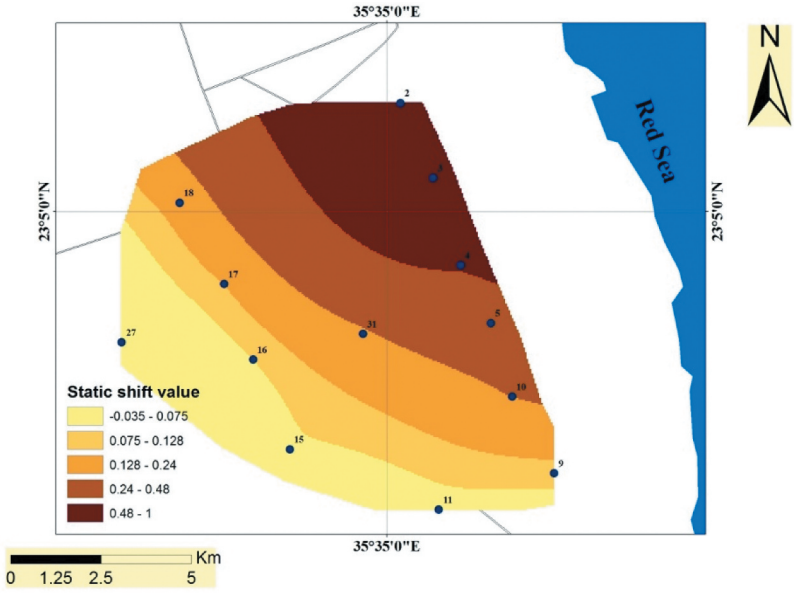

Figure 13. Contour map for the static shift value distribution.

electric current and increases the shifting value in the DC sounding curves. Going to the west, the basement rocks are located at a shallower depth, as the VES method is highly sensitive to the resistive unites so, it might be the reason for decreasing the static shift value. The geological sections (Figure 14 A and B) of VES and TEM data show matched results, especially in the subsurface structure and depth to the basement.

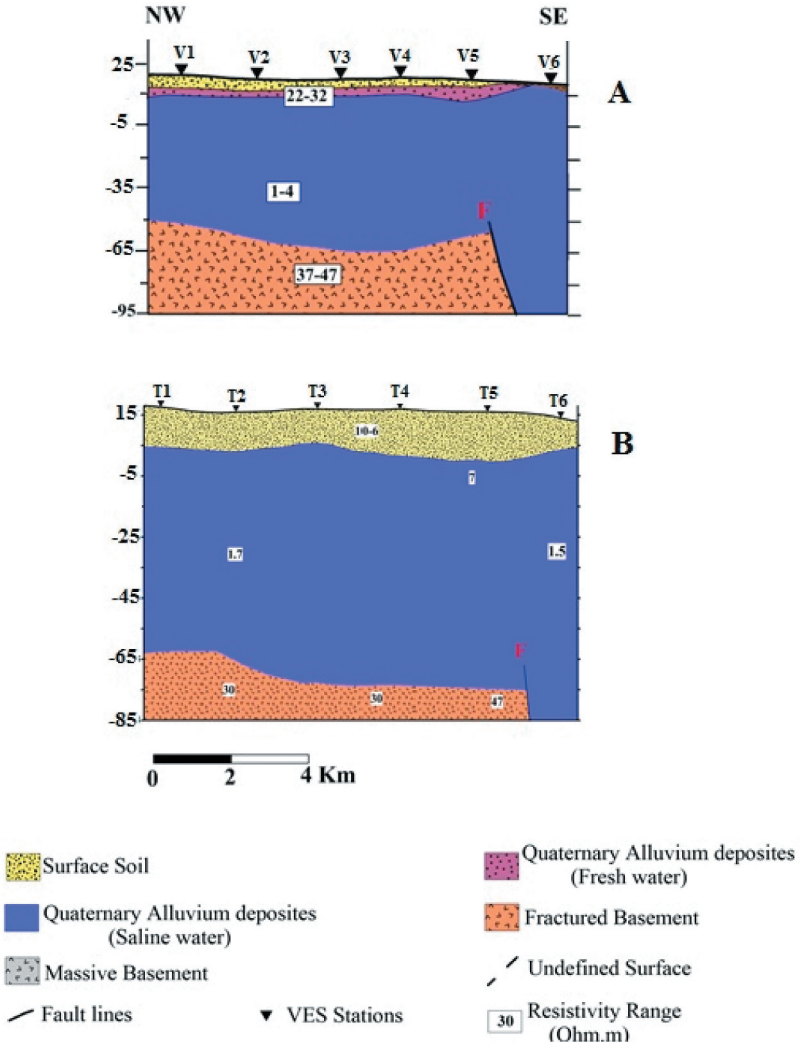

Figure 14. The geoelectrical section. (a) geoelectric section of VES data, (b) geoelectric section of TEM data.

5. Conclusion

Integration between VES and TEM data is used to calculate the shifting value, resulting from the distortion of the electric field caused by shallow and local small bodies of the depositional fan's heterogeneous nature. TEM data not affected by the galvanic distortion as VES data. The removal of that factor from VES data produced a more reliable geological model and matched with the TEM inversion model. Sounding curves for the two data sets at the same location have the same curve pattern (concordant pattern). From 1D models of VES and TEM in Shalateen, both of them are highly matching at the basement depth value after removing the static shift from VES curve. Both models are not matched at shallow subsurface because of differences in vertical resolution between both methods.

Disclosure statement

No potential conflict of interest was reported by the author(s).

Funding

This work was supported by the JSPS KAKENHI [19K13305].

References

Bahr K. 1988. Interpretation of the magnetotelluric impedance tensor: regional induction and local telluric distortion. J Geophys. 62:119–127.

Bahr K. 1991. Geological noise in magnetotelluric data: a classification of distortion types. Phys Earth Planetary Interiors. 66(1–2):24–38. doi:10.1016/0031-9201(91)90101-M.

Baraka AM. 2003. Geologic studies on the Neogene and Quaternary sediments and their bearing on water resources in Shalatein – halaib area, Egypt. Ph D Fac of Sci. 175. El-Azhar University.

Barker R. 1981. THE OFFSET SYSTEM OF ELECTRICAL RESISTIVITY SOUNDING AND ITS USE WITH A MULTICORE CABLE*+. Geophys Prospect. 29 (1):128–143. doi:10.1111/j.1365-2478.1981.tb01015.x.

Barker R. 1992. A simple algorithm for electrical imaging of the subsurface. First Break 10. 53–62.

Beard LP, Tripp AC. 1995. Investigating the resolution of IP arrays using inverse theory. Geophysics. 60 (5):1326–1341. doi:10.1190/1.1443869.

Bortolozo CA, Porsani JL, Santos FAMD, Almeida ER. 2015. VES/TEM 1D joint inversion by using Controlled Random Search (CRS) algorithm. J Appl Geophys Elsevier B V. 112:157–174. doi:10.1016/j.jappgeo.2014.11.014.

Delhaye DR, Rath V, Jones AG, Muller AMR. 2017. Correcting for static shift of magnetotelluric data with airborne electromagnetic measurements: a case study from Rathlin Basin, Northern Ireland. Solid Earth. 8 (3):637–660. doi:10.5194/se-8-637-2017.

El-Belasy IM (1994). *Quaternary geology of some selected drainage basins in upper Egypt (Qena-Edfu area). Ph.D. thesis*, Geology Department, Cairo University, 300 *p*

Flathe H. 1976. The role of a geologic concept in geophysical research work for solving hydrogeological problems. Geoexploration. 14(3–4):195–206. doi:10.1016/0016-7142(76)90013-2.

Flathe H, Leibold W. 1986. The smooth sounding graph a manual for Field Work in Direct Current Resistivity Sounding. Hannover (Germany): Federal institute for geosciences and natural resources; p. 53.

Conoco map:, (1981). Stratigraphic Lexicon and Explanatory Notes to th Geological Map of Egypt. 1: 5000.000. Conoco (Cairo), pp. (1–264).

Hersir GP, Björnsson A, (1991). Geophysical exploration for geothermal resources. Principles and applications. UNU-GTP (Iceland), report pp (15–94).

Massoud U, Qady GE, Metwaly M, Santos F. 2009. Delineation of Shallow Subsurface Structure by Azimuthal Resistivity Sounding and Joint Inversion of VES-TEM Data: case Study near Lake Qaroun, El Fayoum, Egypt. Pure and Applied Geophysics. 166 (4):701–719. doi:10.1007/s00024-009-0463-8.

Meju MA. 2005. Simple relative space-time scaling of electrical and electromagnetic depth sounding arrays: implications for electrical static shift removal and joint DC-TEM data inversion with the most-squares criterion. Geophys Prospect. 53(4):463–479. doi:10.1111/j.1365-2478.2005.00483.x.

Mwakirani R, Simiyu C, Gichira J. 2012. Application of Transient Electromagnetics in Static Shift Correction for Magnetotellurics Data Case Study: paka Geothermal Prospect in Kenya. GRC Transactions. 36:1013–1016.

Park SK. 1985. Distortion of magnetotelluric sounding curves by three-dimensional structures. Geophysics. 50:786–797.

Pellerin L, Hohmann GW. 1990. Transient electromagnetic inversion: a remedy for magnetotelluric static shifts. Geophysics. 55(9):1242–1250. doi:10.1190/1.1442940.

Sadek MF. 2008. Geological and Structural Setting of Wadi Hodein area southeast Egypt with remote sensing applications. The International Archives of the Photogrammetry. Remote Sensing Spatial Information Sci. XXXVII. *Part B8*. (1245-1250)

Said R. 1962. The Geology of Egypt. Elsevier Publishing Company. Amsterdam. Vol. 377.

Spitzer K. 2001. Magnetotelluric static shift and direct current sensitivity. Geophys J Inter. 144(2):289–299. doi:10.1046/j.1365-246x.2001.00311.x.

Stephen J, Gokarn SG, Manoj C, Singh SB. 2003. Effects of galvanic distortions on magnetotelluric data: interpretation and its correction using deep electrical data. Proc Indian Academy of Sci, Earth Planetary Sci. 112 (1):27–36.

Sternberg BK, Washburne JC, Pellerin L. 1988. Correction for the static shift in magnetotellurics using transient electromagnetic soundings. Geophysics. 53 (11):1459–1468. doi:10.1190/1.1442426.

Sultan SA, Santos FM. 2009. Combining TEM/resistivity joint inversion and magnetic data for groundwater exploration: application to the northeastern part of Greater Cairo, Egypt. Environ Geol. 58(3):521–529. doi:10.1007/s00254-008-1527-2.

Tang W, Li Y, Oldenburg DW, Liu J. 2018. Removal of galvanic distortion effects in 3D magnetotelluric data by an equivalent source technique. Geophysics. 83(2):E95–E110. doi:10.1190/geo2016-0668.1.

Yehia IL, El Sayed E, Gomaa Mohammed AA. 2006. Preliminary Hydrogeologic Investigations of Nubia Sandstone and fractured Basement Aquifers in the Area between El Shalateen and Halayeb, Eastern Desert, Egypt, Chapter Uranium in the Environment, Mining Impact and Consequences. Springer Verlag; p. 619–638.

Yousef AF, Salem AA, Baraka AM, Aglan OS. 2009. The impact of geological setting on the groundwater occurrences in some wadis in Shalatein-Abu Ramad Area, south Eastern Desert. Egypt Eur Water. 25(26):s53–68.

Zohdy AA. 1989. A new method for the automatic interpretation of Schlumberger and Wenner sounding curves. Geophysics. 54(2):245–251. doi:10.1190/1.1442648.

Zohdy AA, Eaton GP, Mabey DR. 1974. Application of surface geophysics to ground water investigations. U.S. Geological Survey. Techniques of Water Resources Investigation, Book. 2(Chapter):D1.